

# Calcium Time Course as a Signal for Spike-Timing–Dependent Plasticity

Jonathan E. Rubin,<sup>1,2,3</sup> Richard C. Gerkin,<sup>2,3</sup> Guo-Qiang Bi,<sup>2,3,4</sup> and Carson C. Chow<sup>1,2,3,4,5</sup>

<sup>1</sup>Department of Mathematics, <sup>2</sup>Center for the Neural Basis of Cognition, <sup>3</sup>Center for Neuroscience at University of Pittsburgh, and <sup>4</sup>Department of Neurobiology, University of Pittsburgh, Pittsburgh, Pennsylvania; and <sup>5</sup>Laboratory of Biological Modeling, National Institute of Diabetes and Digestive and Kidney Diseases, National Institutes of Health, Bethesda, Maryland

Submitted 5 August 2004; accepted in final form 6 December 2004

**Rubin, Jonathan E., Richard C. Gerkin, Guo-Qiang Bi, and Carson C. Chow.** Calcium time course as a signal for spike-timing–dependent plasticity. *J Neurophysiol* 93: 2600–2613, 2005. First published December 29, 2004; doi:10.1152/jn.00803.2004. Calcium has been proposed as a postsynaptic signal underlying synaptic spike-timing–dependent plasticity (STDP). We examine this hypothesis with computational modeling based on experimental results from hippocampal cultures, some of which are presented here, in which pairs and triplets of pre- and postsynaptic spikes induce potentiation and depression in a temporally asymmetric way. Specifically, we present a set of model biochemical detectors, based on plausible molecular pathways, which make direct use of the time course of the calcium signal to reproduce these experimental STDP results. Our model features a modular structure, in which long-term potentiation (LTP) and depression (LTD) components compete to determine final plasticity outcomes; one aspect of this competition is a veto through which appropriate calcium time courses suppress LTD. Simulations of our model are also shown to be consistent with classical LTP and LTD induced by several presynaptic stimulation paradigms. Overall, our results provide computational evidence that, while the postsynaptic calcium time course contains sufficient information to distinguish various experimental long-term plasticity paradigms, small changes in the properties of back-propagation of action potentials or in synaptic dynamics can alter the calcium time course in ways that will significantly affect STDP induction by any detector based exclusively on postsynaptic calcium. This may account for the variability of STDP outcomes seen within hippocampal cultures, under repeated application of a single experimental protocol, as well as for that seen in multiple spike experiments across different systems.

## INTRODUCTION

Recent experiments have found that the modification of synaptic strengths in many systems depends on the precise timing of pre- and postsynaptic spikes (Bell et al. 1997; Bi and Poo 1998; Debanne et al. 1998; Magee and Johnston 1997; Markram et al. 1997; Sjöström et al. 2001; Yao and Dan 2001; Zhang et al. 1998). In this spike-timing–dependent plasticity (STDP), if a presynaptic spike precedes a postsynaptic spike within a window of tens of milliseconds, the corresponding synapse potentiates. If a presynaptic spike arrives after a postsynaptic spike within a similar window, the synapse depresses. The details of the signaling mechanism that the synapse uses to detect the timing between pre- and postsynaptic spikes are not fully known (Bi 2002; Bi and Poo 2001; Senn 2002; Sjöström and Nelson 2002).

Calcium has long been suggested as a signaling agent for long-term potentiation (LTP) and depression (LTD) (Lisman 1989; Malenka et al. 1988; Yang et al. 1999) and more recently

STDP (Bi and Poo 2001; Bi and Wang 2002; Sjöström and Nelson 2002). Calcium can enter dendrites through *N*-methyl-D-aspartate (NMDA) channels or local voltage-gated calcium channels (VGCCs). Although there is experimental and modeling support for postsynaptic calcium as a critical signal to initiate molecular mechanisms leading to synaptic plasticity, open questions remain. It is not clear whether a calcium-based mechanism is sufficient to explain all of the experimental data for STDP. It is also uncertain if such a mechanism at the same time accounts for the induction of classical LTP and LTD. Additionally, it is unknown what outcomes such a system would yield for multiple pre- and postsynaptic spikes. We use a combination of computational modeling and experiments to address these questions.

Some recent modeling efforts have considered postsynaptic calcium concentration *levels* as the signal to differentiate pre- and postsynaptic spike orderings and timings (Abarbanel et al. 2003; Karmarkar and Buonomano 2002; Shouval et al. 2002). In these models, high postsynaptic calcium levels lead to LTP and low calcium levels lead to LTD. Models using this hypothesis can capture certain of the phenomena of STDP and/or classical LTP/LTD. They predict, however, that when a presynaptic spike *precedes* a postsynaptic spike by a sufficiently long time interval, calcium levels drop low enough so that the synapse depresses. While one publication reports such a result (Nishiyama et al. 2000), other experiments do not see the effect. Additionally, there is evidence that this second LTD regimen at positive (pre-before-post) timing may be due to feedforward inhibition in the native circuitry (Aihara et al. 2003; Togashi et al. 2003).

In this paper, we show that, for any deterministic signaling system based only on postsynaptic calcium levels, this pre-before-post depression is unavoidable. Furthermore, a level-based system conflicts fundamentally with our experimental results using triplets of pre- and postsynaptic spikes, which indicate that when a presynaptic spike is followed by a postsynaptic spike that is followed by another presynaptic spike (pre-post-pre), there is no change in synaptic strength, whereas the complementary arrangement (post-pre-post) leads to LTP.

As an alternative, we present a model based on the detection of the postsynaptic calcium *time course* (Holthoff et al. 2002; Ismailov et al. 2004; Sabatini et al. 2002; Yang et al. 1999; Yuste et al. 1999) that can reproduce STDP outcomes for spike pairs, triplets, and quadruplets, as well as classical LTD and LTP results induced by repeated presynaptic stimulation (Cho et al. 2001; Dudek and Bear 1992; Wang and Wagner 1999). In

Address for reprint requests and other correspondence: J. Rubin, University of Pittsburgh, Dept. of Mathematics, 301 Thackeray Hall, Pittsburgh, PA 15260 (E-mail: rubin@math.pitt.edu).

The costs of publication of this article were defrayed in part by the payment of page charges. The article must therefore be hereby marked “advertisement” in accordance with 18 U.S.C. Section 1734 solely to indicate this fact.

particular, LTD depends on the width of the calcium signal, namely the durations and relative timings of periods that the calcium signal spends above certain thresholds, interacting nonlinearly. Our model postsynaptic cell is based on the experimentally derived CA1 pyramidal cell model of Poirazi et al. (2003), with synaptic receptor kinetics based on time courses found experimentally (Andrasfalvy and Magee 2001; Perouansky and Yaari 1993), and calibrated to match dendritic calcium profiles reported in the literature (Koester and Sakmann 1998; Murthy et al. 2000; Sabatini et al. 2002). Plasticity in the model is produced by distinct calcium-driven modules for LTD and LTP that interact to determine the final plasticity outcome (Wang et al. 2005). Furthermore, the LTD module includes a *veto*, through which appropriately timed periods of moderate calcium concentration can block LTD components. Plasticity outcomes are determined dynamically, through the evolution of differential equations that are driven by changes in calcium concentration. To our knowledge, this is the first computational model for STDP to fully use the calcium time course, although Abarbanel et al. (2003) have harnessed certain aspects of the calcium time course for reproducing experimental STDP results.

The specific model that we present here represents an example of a general set of components that seem to be necessary to reproduce experimental spike pair and triplet STDP results from hippocampal culture, using postsynaptic calcium dynamics. This is consistent with experimental findings that have uncovered postsynaptic components of STDP in hippocampal culture (Li et al. 2004; Wang et al. 2005); since specific presynaptic components (e.g., Sjöström et al. 2003) have not been implicated in this preparation, these are not included in the model. Our computational results indicate that any model that aims to reconcile the pair and triplet data using the postsynaptic calcium signal alone will require some amount of fine-tuning. Consistency with classical LTP/LTD further constrains any model. The inherent sensitivity of a calcium-based detection system may contribute both to the variability in plasticity outcomes induced by certain experimental protocols and to the disparity in results of triplet experiments in different experimental settings (Froemke and Dan 2002; Sjöström et al. 2001; Wang et al. 2005).

## METHODS

### *Cell culture and electrophysiology*

Low-density cultures of dissociated embryonic rat hippocampal neurons were prepared according to a previously described protocol with minor modifications (Bi and Poo 1998). Hippocampi were removed from E17–E19 embryonic rats and treated with trypsin for 20 min at 37°C, followed by washing and gentle trituration. The dissociated cells were plated on poly-L-lysine-coated glass coverslips in 35-mm petri dishes with 30,000–90,000 cells per dish. The culture medium was Dulbecco's modified Eagle's medium (DMEM; BioWhittaker) supplemented with 10% heat-inactivated bovine calf serum (Hyclone), 10% Ham's F12 with glutamine (BioWhittaker), and 50 U/ml penicillin-streptomycin (Sigma). Twenty-four hours after plating, one-third of the culture medium was replaced by the same medium supplemented with 20 mM KCl. Both glial cells and neurons grow well under these culture conditions. The optimal period for these cultures to be used is 8–15 div (days in vitro), during which connections of 50–500 pA were commonly found. Very strong synapses (>500 pA) in these cultures express little LTP (Bi and Poo 1998) and were excluded from the study.

Simultaneous whole cell perforated-patch recordings from two glutamatergic neurons were carried out with patch-clamp amplifiers (Axopatch 200B, Multiclamp 700A, Axon Instruments) at room temperature. The pipette solution contained the following (in mM): 136.5 potassium gluconate, 17.5 KCl, 9 NaCl, 1 MgCl<sub>2</sub>, 10 HEPES, 0.2 EGTA, and 200 μg/ml amphotericin B (pH 7.3). The external bath solution was a HEPES-buffered saline (HBS) containing the following (in mM): 150 NaCl, 3 KCl, 3 CaCl<sub>2</sub>, 2 MgCl<sub>2</sub>, 10 HEPES, and 5 glucose (pH 7.3). Throughout the recording, the culture was perfused with fresh bath medium at a rate of ~2 ml/min, using an automated perfusion system (VC64, Warner Instrument) that allows for rapid change of solutions. The neurons were visualized with a phase-contrast inverted microscope (Leica DMIRB). Signals (filtered at 5 kHz) were acquired at a sampling rate of 10 kHz using a 16-bit digitizing board (DigiData1320, Axon Instruments or E6035, National Instruments) interfaced with either pClamp8 software (Axon Instruments) or a LabView-based customized program recently developed in our laboratory. Series resistances and input impedance were monitored by a test hyperpolarizing pulse (5 mV, 10 ms). In general there was no significant change in series resistance (10–30 MΩ) and input impedance (300–500 MΩ) following repetitive pairing protocols. Data were accepted for analysis only in the cases where series resistance and input impedance did not vary beyond 10% throughout the experiment. Trials showing significant run-up or run-down during the control period (>5% over 10 min) were also excluded from further analysis. Recorded excitatory postsynaptic current (EPSC) traces were analyzed using the pClamp program (Axon Instruments). STDP ratio was calculated from the averaged EPSC amplitude within 10 min before and that between 15 and 30 min after the stimulation paradigm.

### *Two-compartment CA1 neuron model*

We used a two-compartment CA1 model consisting of a soma and a localized dendritic region, which allowed for consideration of back-propagation of action potentials initiated experimentally in the soma. The starting point for our model was the experimentally calibrated multi-compartment CA1 pyramidal cell model developed by Poirazi et al. (2003). We reduced the model to two compartments in a way such that the voltage dynamics in the single dendritic region qualitatively matched those in a typical dendritic compartment of Poirazi et al. (2003). In the rest of the paper, we refer to the dendritic compartment in our model as a "spine" to represent the fact that we assume that there is minimal calcium diffusion out of this compartment (Goldberg et al. 2003; Sabatini et al. 2002) and that calcium is well-mixed throughout the compartment (Kovalchuk et al. 2000; Murthy et al. 2000; Sabatini et al. 2002). However, it should be noted that true spines are not well-developed in rat hippocampal cultures. We further reduced the model by systematically removing conductances that did not significantly affect voltage dynamics in response to current injections or to synaptic inputs; the reduced and full two-compartment models yield similar calcium time courses. We also replaced the calcium dynamics of the Poirazi et al. (2003) model with a modified version of those of Traub et al. (1994) to replicate the calcium profiles reported in Koester and Sakmann (1998), Yuste et al. (1999), Murthy et al. (2000), and Sabatini et al. (2002). Furthermore, we used the more natural form of kinetic equations for current activations and inactivations given in Traub et al. (1994)

$$z' = \alpha_z(v)(1 - z) - \beta_z(v)z \quad (1)$$

where  $z$  denotes the dimensionless activation or inactivation variable and  $v$  is the membrane voltage of the appropriate compartment. The activation and inactivation functions, denoted  $\alpha_z(v)$ ,  $\beta_z(v)$  in Eq. 1, are still from Poirazi et al. (2003). Note that in Eq. 1 and all subsequent equations, differentiation is with respect to time.

The ordinary differential equations for the voltage potentials in the compartments in the reduced model take the form

$$v' = (I_L + I_{Na} + I_K + I_{Ca} + I_{coup} + I_{in})/C_m \quad (2)$$

where  $I_L$  denotes a leak current;  $I_{Na}$  denotes a sodium current;  $I_K$  corresponds to the sum of a potassium A current ( $I_A$  in Poirazi et al. 2003), a delayed rectifier potassium current ( $I_{Kdr}$  in Poirazi et al. 2003), and a calcium-activated potassium afterhyperpolarization current ( $I_{mAHP}$  in Poirazi et al. 2003);  $I_{Ca}$  is a high-threshold calcium current ( $I_{CaL}$  in Poirazi et al. 2003);  $I_{coup}$  denotes the electrical coupling between the compartments in  $\mu A/cm^2$ , given by  $I_{coup} = 1.125(v_i - v_j)$  in the equation for compartment  $i$ ; and  $I_{in}$  corresponds to current injections (in the soma) or to AMPA and NMDA synaptic currents,  $I_{syn,AMPA}$  and  $I_{syn,NMDA}$  (in the spine). The forms of these currents are specified in Poirazi et al. We normalized the membrane capacitance  $C_m$  to  $1 \mu F/cm^2$  and we modified the conductances of these currents to maintain appropriate voltage dynamics in our compartmental reduction; the values used (in  $mS/cm^2$ ) appear in Table 1.

As mentioned above, we use a modified version of the calcium equations from Traub et al., which take the form

$$\begin{aligned} \chi'_{soma} &= \Phi I_{Ca,soma} - \beta_{soma}(\chi_{soma} - \chi_{0,soma}) + (\chi_{spine} - \chi_{soma})/d - (\beta_{soma}/n_{buff})\chi_{soma}^2 \\ \chi'_{spine} &= \Phi(I_{Ca,spine} + I_{Ca,NMDA}) - \beta_{spine}(\chi_{spine} - \chi_{0,spine}) \\ &\quad - (\beta_{spine}/n_{buff})\chi_{spine}^2 - \beta_{buff}\chi_{spine} \quad (3) \end{aligned}$$

where, for  $x$  in the set {soma, spine}, the term  $\chi_x$  denotes calcium concentration in micromolar,  $\chi_{0,x}$  denotes the baseline resting calcium level,  $d$  relates to the calcium diffusion rate from the soma to the spine, and  $n_{buff}$  controls the strength of nonlinear calcium buffering, whereas  $\beta_{buff}$  scales a linear buffering term. The currents  $I_{Ca,soma}$  and  $I_{Ca,spine}$  in Eq. 3 denote VGCC terms (as in Eq. 2), with  $\Phi$  denoting a factor to convert from units of current to units of concentration, itself depending on buffering. We take  $\Phi$  to have magnitude 0.01 for both compartments, which reflects similar volumes of active zones, independent of overall compartmental volumes. The other parameters here are  $\beta_{soma} = \beta_{spine} = 0.083/ms$ ,  $\chi_{0,soma} = 0.05 \mu M$ ,  $\chi_{0,spine} = 0.07 \mu M$ ,  $d = 1,000$  ms,  $n_{buff} = 6$ , and  $\beta_{buff} = 0$ . These parameters were selected to match experimental data on dendritic calcium dynamics (Koester and Sakmann 1998; Murthy et al. 2000; Sabatini et al. 2002; Yuste et al. 1999), with resting calcium in particular constrained by specific experimental results (Maravall et al. 2000; Pozzo-Miller et al. 1999; Yuste et al. 1999).

The current flow through NMDA channels includes several different ion types. For the calcium current through the NMDA channels in the spine, denoted  $I_{Ca,NMDA}$  in Eq. 3, and the total current through these NMDA channels, which we denote  $I_{syn,NMDA}$ , we used equations of the form

$$I_{x,NMDA} = -g_{x,NMDA} s_{NMDA} m_{x,NMDA} (v_{spine} - v_{x,rev}) \quad (4)$$

for  $x$  in the set {Ca, syn}. In Eq. 4,  $g_{x,NMDA}$  denotes the channel conductance to the appropriate current,  $s_{NMDA}$  is the activation level of the NMDA channels,  $m_{x,NMDA}$  measures the extent of removal of magnesium block of the appropriate ionic flow, and  $v_{x,rev}$  is the reversal potential of the calcium current, namely 140 mV, or of the total current through the NMDA channels, namely 0 mV. We set

TABLE 1. Conductances used in the two-compartment CA1 model

Parameter	Value in Soma, mS/cm <sup>2</sup>	Value in Spine, mS/cm <sup>2</sup>
$g_L$	0.1	0.1
$g_{Na}$	30	7
$g_{K(A)}$	7.5	12
$g_{K(dr)}$	14	0.867
$g_{K(mAHP)}$	25	0
$g_{Ca(L)}$	7	25

$g_{Ca,NMDA} = 25$  mS/cm<sup>2</sup> and  $g_{syn,NMDA} = 0.3$  mS/cm<sup>2</sup> (although this can be made much smaller with no qualitative effect). From Jahr and Stevens (1990, 1993), we use

$$m_{syn,NMDA} = 1.0[1.0 + 0.3(Mg) \exp(-0.062v_{spine})]$$

$$m_{Ca,NMDA} = 1.0[1.0 + 0.3(Mg) \exp(-0.124v_{spine})]$$

with  $Mg = 2$  mM.

The AMPA synaptic current is given by

$$I_{syn,AMPA} = -g_{AMPA} s_{AMPA} (v_{spine} - v_{syn,rev})$$

with  $g_{AMPA} = 0.05$  mS/cm<sup>2</sup>. For both the NMDA and AMPA currents, we used activation equations designed to give stimulus-induced synaptic current time courses that compare favorably with biological experiments at room temperature (Andrasfalvy and Magee 2001; Perouansky and Yaari 1993). These take the form

$$s_x = s_{x,fast} + s_{x,slow} + s_{x,rise} \quad (5)$$

where  $x$  in the set of {NMDA, AMPA} and where we took

$$s'_{NMDA,rise} = -\Phi_{NMDA}(1 - s_{NMDA,fast} - s_{NMDA,slow})f_{pre}(t) - s_{NMDA,rise}/\tau_{NMDA,rise}$$

$$s'_{NMDA,fast} = \Phi_{NMDA}(0.527 - s_{NMDA,fast})f_{pre}(t) - s_{NMDA,fast}/\tau_{NMDA,fast}$$

$$s'_{NMDA,slow} = \Phi_{NMDA}(0.473 - s_{NMDA,slow})f_{pre}(t) - s_{NMDA,slow}/\tau_{NMDA,slow}$$

and

$$s'_{AMPA,rise} = -\Phi_{AMPA}(1 - s_{AMPA,fast} - s_{AMPA,slow})f_{pre}(t) - s_{AMPA,rise}/\tau_{AMPA,rise}$$

$$s'_{AMPA,fast} = \Phi_{AMPA}(0.903 - s_{AMPA,fast})f_{pre}(t) - s_{AMPA,fast}/\tau_{AMPA,fast}$$

$$s'_{AMPA,slow} = \Phi_{AMPA}(0.097 - s_{AMPA,slow})f_{pre}(t) - s_{AMPA,slow}/\tau_{AMPA,slow}$$

The parameters for these equations are  $[\Phi]_{NMDA} = 20/ms$ ,  $\tau_{NMDA,rise} = 2$  ms,  $\tau_{NMDA,fast} = 10$  ms,  $\tau_{NMDA,slow} = 45$  ms,  $[\Phi]_{AMPA} = 20/ms$ ,  $\tau_{AMPA,rise} = 0.58$  ms,  $\tau_{AMPA,fast} = 7.6$  ms, and  $\tau_{AMPA,slow} = 25.69$  ms. Note that  $f_{pre}(t)$  represents a step pulse that is turned on to initiate the postsynaptic effect when a presynaptic spike occurs.

### Calcium detectors

The mechanism for plasticity in our model involves a biophysically plausible calcium detection system that responds to calcium and then changes the strength of the synapse accordingly. In the model, three detector agents ( $P$ ,  $A$ ,  $V$ ) respond to the instantaneous calcium level in the spine compartment. The interactions of these three agents, together with two others ( $D$ ,  $B$ ) that they influence, act to track the calcium time course in the spine (see Fig. 3A). More specifically, different calcium time courses lead to different time courses of  $P$  and  $D$ , which compete to influence a plasticity variable  $W$ . This variable  $W$  is used as a measure of the sign and magnitude of synaptic strength changes from baseline. Note that this scheme is significantly different from a detection of peak calcium levels, in which the change in  $W$  would be determined by how large spine calcium becomes during an appropriate set of spikes. The interactions between agents within our detector system qualitatively resemble the pathways influencing the regulation of  $Ca^{2+}$ /calmodulin-dependent protein kinase II (CaMKII) (Bhalla and Iyengar 1999; Lisman 2001).

The detector equations are

$$P' = (p_\sigma(\chi_{spine}) - c_p AP)/\tau_p$$

$$V' = (v_\sigma(\chi_{spine}) - V)/\tau_v$$

$$A' = (a_\sigma(\chi_{spine}) - A)/\tau_a$$

$$B' = (b_\sigma(A) - B - c_d BV)/\tau_b$$

$$D' = (d_\sigma(B) - D)/\tau_d$$

$$W' = \{\alpha_w/[1 + \exp((P - p)/k_p)] - \beta_w/[1 + \exp((D - d)/k_d)] - W\}/\tau_w \quad (6)$$

For a biologically relevant form of calcium sensitivity in  $P$  and  $A$ , we use the Hill equations

$$p_{\sigma}(x) = \frac{10(x/pHC)^{pHN}}{1 + (x/pHC)^{pHN}}$$

and

$$a_{\sigma}(x) = \frac{(x/aHC)^{aHN}}{1 + (x/aHC)^{aHN}}$$

with Hill coefficients (with respect to calcium) taken from previous modeling work on the activation, autophosphorylation, and dephosphorylation of CaMKII (Holmes 2000; Lisman and Zhabotinsky 2001). We set

$$f_{\sigma}(x) = \alpha_f / [1.0 + \exp((x - \theta_f)/\sigma_f)]$$

for  $f$  in the set  $\{v, d, b\}$ . The relevant parameters appear in Table 2.

Note that  $P$  detects calcium levels that exceed the threshold of 4  $\mu\text{M}$  (i.e., high calcium). The results of Bradshaw et al. (2003) suggest that the presence of protein phosphatase 1 (PP1) can influence the steady-state calcium sensitivity of CaMKII. We included an analogous effect through the weak competition term  $c_p\text{AP}$  term in the  $P$  equation, although one could alternatively choose to alter the Hill equation for  $P$  to obtain similar results.  $A$  detects calcium levels that exceed the lower threshold of 0.6  $\mu\text{M}$ , and its fast time constant ensures that the time course of  $A$  follows that of calcium rather closely, but with some smoothing out of peaks and valleys. If a postsynaptic spike precedes a presynaptic input by a small  $\Delta t$ , then  $A$  accumulates over both, reaching a threshold for the activation of  $B$ . This double-filter acts as a width detector for the calcium concentration. If enough of  $B$  accumulates, then  $D$  is activated. This double-filter system also eliminates depression from post-pre pairings with  $\Delta t$  outside of the appropriate depression window. There may be other ways to achieve these effects but our analysis suggests that the elements of width detection and modular competition are essential (see RESULTS).

Sufficiently large  $P$  values increase  $W$ , while sufficiently large  $D$  decreases  $W$ , setting up a potential second, more significant, competition between potentiation and depression, beyond the  $c_p\text{AP}$  term in the  $P$  equation, which ensues if the mechanisms for both are activated. Like  $P$  and  $A$ , the variable  $V$  responds to a calcium threshold, namely 2  $\mu\text{M}$ , and its fast time constant gives close tracking of calcium level.  $V$  acts as a "veto" on the accumulation of  $B$ , through the competitive term  $c_d\text{BV}$  in the  $B$  equation. This veto prevents calcium levels that are sustained near or above 2  $\mu\text{M}$  from activating the LTD side of the  $W$  equation. The existence of such an interaction is motivated by the inhibitory effect of protein kinase A (PKA) on PP1, but it represents the integrated effect of many pathways, with an effective threshold set by our choice of  $v_{\sigma}(\chi_{\text{spine}})$ . The LTD block that the veto provides is

TABLE 2. Parameters appearing in the calcium detector equations

Parameter	Value	Parameter	Value
$pHC$	4 $\mu\text{M}$	$pHN$	4
$aHC$	0.6 $\mu\text{M}$	$aHN$	3
$\theta_v$	2 $\mu\text{M}$	$\sigma_v$	-0.05
$\theta_d$	2.6	$\sigma_d$	-0.01
$\theta_b$	0.55	$\sigma_b$	-0.02
$\tau_p$	500 ms	$k_p$	-0.1
$\tau_a$	5 ms	$k_d$	-0.002
$\tau_v$	10 ms	$\alpha_v$	1.0
$\tau_d$	250 ms	$\alpha_d$	1.0
$\tau_b$	40 ms	$\alpha_b$	5.0
$c_p$	5	$c_d$	4
$\tau_w$	500 ms	$p$	0.3
$\alpha_w$	0.8	$d$	0.01
$\beta_w$	0.6		

relevant for pre-post spike pairings, as well as for post-pre-post triplet experiments and for classical LTP/LTD.

### Simulations

All simulations were performed using the software XPPAUT (Ermentrout 2002). We used the fourth-order Runge-Kutta method for numerical integration in XPPAUT, with a step size of  $\delta t = 0.025$  ms.

### RESULTS

We performed a number of numerical experiments on our conductance-based CA1 model neuron, consisting of a spike-generating somatic compartment and a dendritic compartment. The latter compartment contains active channels and represents an isolated synaptic region such as a spine. Similar results were obtained with a more comprehensive, four-compartment model, featuring separate compartments for the soma, a dendrite, a spine, and a postsynaptic density within a spine. In the model, calcium influx through NMDA channels depends on the level of magnesium block, which is affected by incoming excitatory postsynaptic potentials (EPSPs) and back-propagating action potentials (BPAPs). VGCCs are activated by the arrival of BPAPs; these are initiated in the soma, but their ability to propagate to the dendritic compartment in part depends on recent activity there. Both of these calcium sources are sensitive to the timing of recent pre- and postsynaptic spikes. We emulated STDP and classical LTP/LTD paradigms with this model.

In the model, the calcium concentrations in the spine resulting from pre- or postsynaptic (somatic) suprathreshold stimulation alone do not elicit plasticity. After presynaptic stimulation, a small amount of calcium enters through the NMDA channels. The AMPA channels induce a limited depolarization, which provides a small relief of magnesium block. With postsynaptic stimulation alone, calcium enters through VGCCs only.

#### *Calcium time courses, but not necessarily levels, differ across paired stimulation protocols*

In a paired protocol of a presynaptic stimulation followed by a postsynaptic stimulation 10 ms later (pre-10-post), we see a large influx of calcium through the NMDA channel due to the removal of the magnesium block by the BPAP (Fig. 1A). In the pre-40-post scenario, the influx of calcium is reduced because the arrival of the BPAP at the dendrite comes later. While the slow closing of the NMDA channels still allows calcium influx to be enhanced by this unblocking, the peak calcium level is lower in the pre-40-post scenario than in pre-10-post (Fig. 1A) because NMDA channels are more inactivated by the time the magnesium block is removed. The peak calcium level will continue to decrease as the pre-post interstimulus interval is lengthened. This inevitable reduction in calcium level will necessarily lead to a zone of pre-post depression in any model that attributes potentiation to high calcium levels and depression to lower calcium levels, independent of where the levels are set.

For a post-before-pre synaptic pairing with a 10-ms interval (post-10-pre), a much smaller level of calcium enters the dendrite, with a different time course (Fig. 1B) than in pre-10-post; most of this calcium comes through L-type VGCCs. The

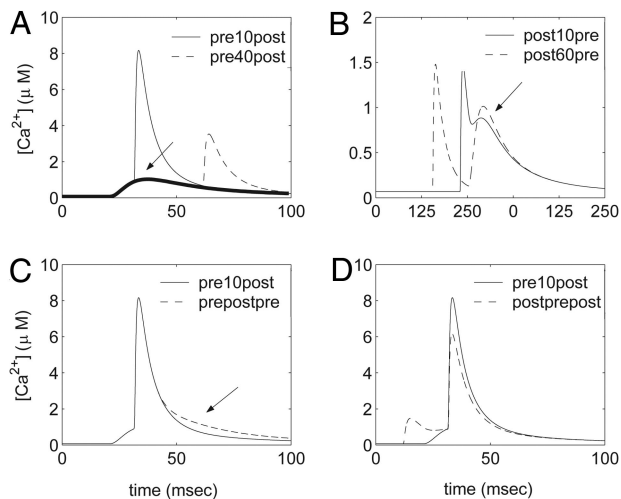


FIG. 1. Postsynaptic calcium profiles. *A*: bold solid curve shows the calcium time course resulting from presynaptic stimulation alone, the other solid curve corresponds to pre-10-post, and the dashed curve is from pre-40-post (which coincides with pre-alone initially). Times shown are measured relative to the start of repeated stimulation experiments. *B*: solid (dashed) curve corresponds to post-10-pre (post-60-pre). Note the different time and calcium scales relative to *A*. The 2nd calcium peak in post-60-pre, marked by the arrow, is almost identical to the pre-alone calcium time course marked with the arrow in *A*, which shows how the scales of *A* and *B* compare. *C*: solid (dashed) curve corresponds to pre-10-post (pre-post-pre). Arrow points out the higher shoulder during calcium decay in pre-post-pre. *D*: solid (dashed) curve corresponds to pre-10-post (post-pre-post).

calcium influx is increased in amplitude (slightly) and duration relative to postsynaptic stimulation alone, because residual dendritic depolarization from the BPAP enhances calcium influx through NMDA channels after presynaptic stimulation. Peak calcium levels are approximately the same for post-60-pre as for post-10-pre, despite the longer interstimulus interval; in fact, the decay of afterhyperpolarization in post-60-pre allows for more calcium influx through NMDA channels than seen in the post-10-pre case. However, the total amount of contiguous time during which the calcium level exceeds  $0.6 \mu\text{M}$  is shorter for the 60-ms interval. In particular, the calcium concentration rises above  $0.6 \mu\text{M}$  briefly after the postsynaptic spike in the post-60-pre simulation and again after the presynaptic stimulation, but a “valley” during which calcium lies below  $0.6 \mu\text{M}$  separates these peaks. It is important to observe that, although there is a range of pre-post interstimulus intervals that will yield similar peak calcium levels to these post-pre results, the calcium time courses of the pre-post and post-pre scenarios are quite distinct.

Note that when paired stimulation is applied repeatedly at 1 Hz, calcium decays to very low levels between pairs. Thus each pairing induces a postsynaptic calcium response that is quite similar to the ones shown for single pairings. The same applies with triplet combinations of pre- and postsynaptic stimulation (Fig. 1, *C* and *D*).

#### Hippocampal culture triplet experiments do not support calcium level detection

Previous studies showed that in hippocampal cultures, LTP could be induced when a post-pre spike pair was followed by a third, postsynaptic spike resulting from a suprathreshold EPSP (Bi and Poo 1998). To examine further the plasticity

outcomes of prescribed spike triplets, we performed experiments in hippocampal cultures. These experiments revealed an interesting asymmetry in the resulting STDP (Fig. 2). Consistent with our previous results, post-pre-post triplets, with 10-ms intervals between all successive stimuli, result in potentiation. On the other hand, pre-post-pre triplets, again with 10-ms intervals between stimuli, result in no consistent change. This is surprising because the calcium influxes resulting from the two triplet patterns are similar. Figure 1, *C* and *D*, shows the calcium time courses for pre-post-pre and post-pre-post stimulation triplets with 10-ms intervals between all successive stimuli. These are compared with the calcium time course for the pre-10-post paradigm. Note that the peak calcium levels shown in Fig. 1, *C* and *D*, in both triplet cases are approximately the same as that for the pre-10-post case, with the peak level in the post-pre-post scenario actually slightly below that for pre-10-post, due to the potassium A current. Since calcium levels do not build up over subsequent triplets, if calcium level alone were used as a signal to select a direction of synaptic plasticity, the prediction would be that potentiation would arise in both cases, with greater potentiation in pre-post-pre than in post-pre-post. This is in complete contrast to what we observe in experiments (Fig. 2), although such behavior has been reported in a different experimental system (Sjöström et al. 2001) and is discussed further below.

#### Features of a calcium time course detector

The similarity of the calcium profiles across pre-post, post-pre, and triplet scenarios (Fig. 1) implies that, to reproduce our experimental plasticity results (Fig. 2, Bi and Poo 1998), any detector based exclusively on calcium must use the entire calcium time course. From an examination of the calcium time

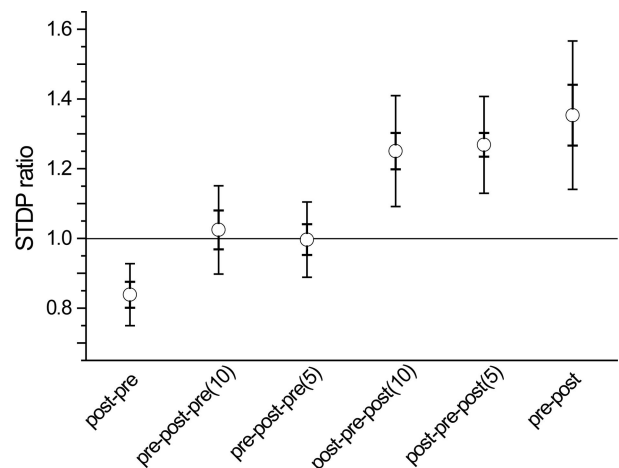


FIG. 2. Summary of experimental spike-timing-dependent plasticity (STDP) induction in hippocampal culture with different stimulation paradigms. Each paradigm consists of spike pairs or triplets that were repeatedly applied to the pre- and postsynaptic neurons, 60 times at 1 Hz. Data points show the mean (squares), SD (thin error bars), and SE (thick error bars). For triplets, the intervals between pre- and postsynaptic spikes were either  $\pm 10$  or  $\pm 5$  ms. Experiments using paired spiking with spike timings ranging from  $-21$  to  $-4$  ms were included in “post-pre.” Experiments with spike timings ranging from  $+9$  to  $+11$  ms were included in “pre-post.” The STDP ratio for each experiment was calculated by dividing the averaged excitatory postsynaptic current (EPSC) amplitude measured within 10 min before the stimulation paradigm by that measured between 15 and 30 min after the stimulation paradigm.

courses in Fig. 1 and the experimental results in Fig. 2, we surmise that a detection system should incorporate three features: 1) calcium levels above a high-threshold (e.g.,  $4 \mu\text{M}$ ; see Fig. 1A) trigger potentiation; 2) levels that exceed a low threshold (e.g.,  $0.6 \mu\text{M}$ ) and remain above for a minimum continuous time (e.g., 45 ms) trigger depression (i.e., the width of the calcium signal must be accounted for; see Fig. 1B); and 3) levels exceeding a mid-level threshold (e.g.,  $2 \mu\text{M}$ ) trigger a veto of the depression components of the model. In particular, with such a veto in place, the relative timings and durations of periods of low and moderate calcium become relevant to the plasticity outcome, enhancing the dependence of plasticity on aspects of the calcium time course other than levels.

As a specific example of a model showing that these features are sufficient for distinguishing STDP scenarios, we constructed a calcium time course detector consisting of five interacting elements together with a readout variable, all described by ordinary differential equations. We do not imply that this implementation is the only or even the optimal way to codify our rules. This merely represents a straightforward possibility using simple chemical kinetics. The interactions of the model's components are shown in Fig. 3A, whereas the actual model equations, with a description of their actions, are given in METHODS. The equations can be viewed as incorporating relatively independent early signaling modules for LTD and for LTP, as recently suggested on the basis of experimental results (Wang et al. 2005). For simplicity, we assume that changes in synaptic strengths are proportional to changes in the readout variable ( $W$ ) and that the effects of the potentiation ( $P$ ) and depression ( $D$ ) components on  $W$  sum linearly. Thus if both are activated at appropriate levels, they can cancel each other. Temporal details of the calcium time course determine the relative strengths of the potentiation and depression components, and hence the state attained by the readout. Figure 3B summarizes the saturation levels, denoted by  $W_\infty$ , of  $W$  for various fixed levels of  $P$  and  $D$ . Note that the evolution of  $W$  is sensitive to  $P$  and  $D$  on much different scales. These scales are completely arbitrary and could be changed by a rescaling of  $D$ ; we left the scales disparate for ease of visualization in Fig. 7D.

Our detector system is inspired by the biomolecular pathways of protein phosphorylation and dephosphorylation (Bhalla and Iyengar 1999; Holmes 2000; Lisman 1994; Lisman and Zhabotinsky 2001; Lisman et al. 2002; Malenka et al. 1989; Malinow et al. 1989; Mulkey et al. 1994; Zhabotinsky 2000). The potentiation detector is motivated by the phosphorylation cascade of CaMKII. The depression detector is a hypothesized abstraction of the kinetics of dephosphorylation agents such as PP1. While it is not our intention to model particular detector variables as direct representatives of particular molecules, experimentally deduced Hill coefficients (with respect to  $\text{Ca}^{2+}$ ) relevant for the phosphorylation and dephosphorylation of CaMKII were used (Holmes 2000; Lisman and Zhabotinsky 2001), supplying each differential equation with a biophysically plausible calcium sensitivity. The veto system is motivated by the competition of kinases and phosphatases, specifically the action of PP1 inhibitory agents such as PKA (e.g., Bhalla and Iyengar 1999; Lee et al. 2000). We stress that the precise form of the detector is unimportant as long as it incorporates the three proposed features. The model developed

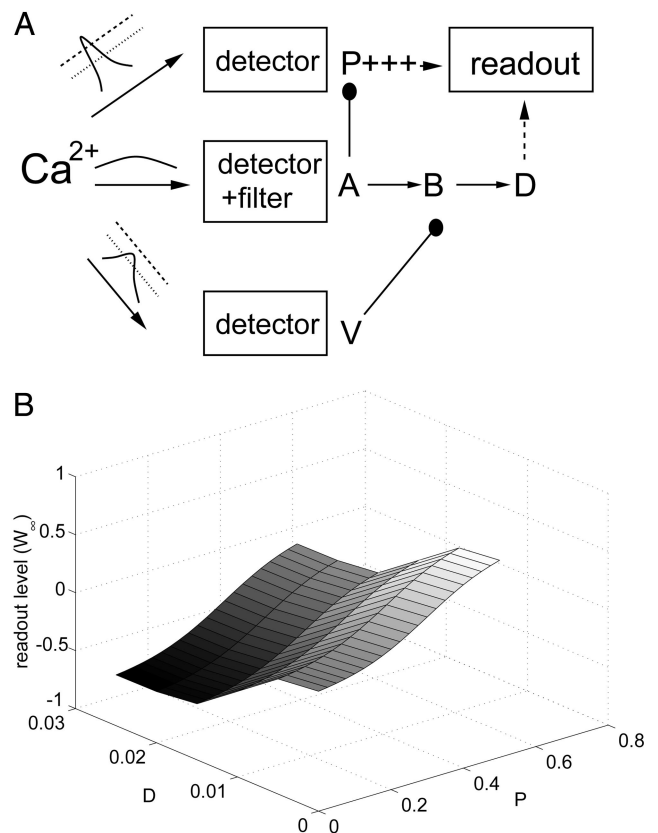


FIG. 3. Calcium detector system. *A*: different components of the system respond to different forms of calcium signals. These components interact, and the outcome of their interactions drives the evolution of the readout variable  $W$ , which is increased by  $P$  and decreased by  $D$ . Connections with solid circles denote suppression of one element by another. Connections with arrows denote relations in which one element turns on another when it reaches a threshold. *B*: saturation levels ( $W_\infty$ ) of the readout variable  $W$  from the calcium detector model. To generate this plot, the potentiation variable  $P$  and the depression variable  $D$  were fixed at various levels, and the  $W$  equation was allowed to evolve until it became asymptotically close to its steady state. Note that  $W_\infty$  increases with  $P$  and decreases with  $D$ , with nonlinear dependencies. Also note the difference in the scales of  $P$  and  $D$ .

here is given to demonstrate that these features are sufficient to reproduce plasticity outcomes in a variety of experimental paradigms.

#### *Plasticity outcomes match experiments and derive from detector responses to calcium time course*

To compare the plasticity outcomes from our calcium time course detection system to experiments on stimulus pairs and triplets, we examine the saturation levels ( $W_\infty$ ) of the readout variable  $W$  in response to simulations of experimental stimulus paradigms. The detector is able to reproduce the STDP window of Bi and Poo (1998) as well as our triplet results (Fig. 2), while giving no plasticity for isolated pre- and postsynaptic spikes (data on isolated spikes not shown). Figure 4 displays the cumulative plasticity results for spike pairing simulations of our full model system, together with previously published data from spike pairing experiments (Bi and Poo 1998). In these simulations, the postsynaptic cell was induced to fire by current injection at a time  $\Delta t$  after the presynaptic cell was stimulated. Note that negative  $\Delta t$  values correspond to post

before pre, whereas positive  $\Delta t$  values correspond to pre before post. For each  $\Delta t$ , the experiment was repeated at 1 Hz until saturation, typically requiring about 20 pairings. Even in the saturated state,  $W$  may oscillate slowly about a fixed level, and accordingly, the  $W_\infty$  levels shown in Fig. 4 were generated by averaging  $W$  over a 1-s period. We stress that this model does not yield depression in pre-post scenarios with large interstimulus intervals, as occurs in previously published models based on calcium levels (Abarbanel et al. 2003; Karmarkar and Buonomano 2002; Shouval et al. 2002).

We can understand how the detector system distinguishes different stimulation scenarios by examining the responses of its components to the corresponding calcium signals. Figure 5 summarizes the responses of some components of our model calcium detector system to single spike pairs in the pre-post stimulation scenarios after transient effects dependent on initial conditions have decayed away. Figure 5A shows the time courses of calcium in the pre-10-post and pre-40-post cases, as in Fig. 1A. In the model, increases in the calcium level detector  $P$  lead to growth of the readout variable  $W$ , corresponding to potentiation, and the responses of  $P$  to these two scenarios are shown in Fig. 5C. Only the larger response is sufficient to cause an observable increase in  $W$ . Figure 5B shows a magnified view of the calcium time course from the pre-40-post simulation. In this case, Fig. 5D shows that, in our model, the depression agents do not build up sufficiently to induce depression. Similar results occur for larger interstimulus intervals (see Fig. 4). The mechanism in our model that prevents depression in the pre-40-post case is the presence of the veto, which is activated by moderate calcium levels. In pre-40-post, there is sufficient calcium influx to activate the veto for a certain period, during which it blocks the build-up of the intermediate depression components of the model. When the veto wears off, there is still enough calcium to cause some increase of the intermediate depression agents, but they cannot increase sufficiently to cause depression (Fig. 5D).

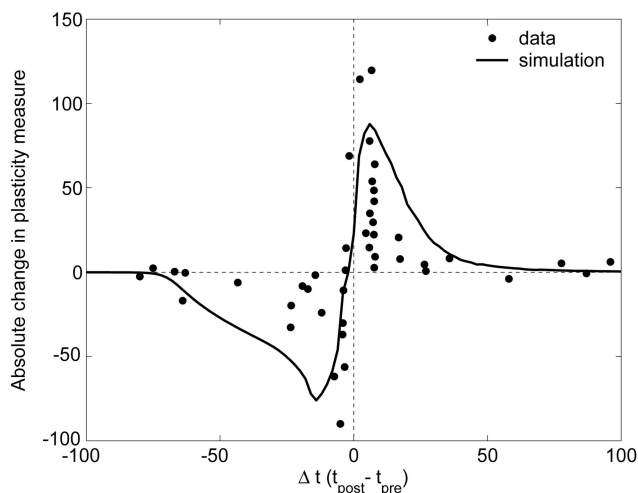


FIG. 4. Plasticity outcomes from spike pair simulations and experiments with interspike intervals  $\Delta t = t_{\text{post}} - t_{\text{pre}}$ . Simulations were performed with  $\Delta t$  ranging from  $-100$  to  $100$ , in increments of  $2$  ms. Solid curve interpolates resulting saturation levels of  $W_\infty$ . Experimental data points (Bi and Poo 1998), marked with circles, represent percent changes in excitatory postsynaptic currents.

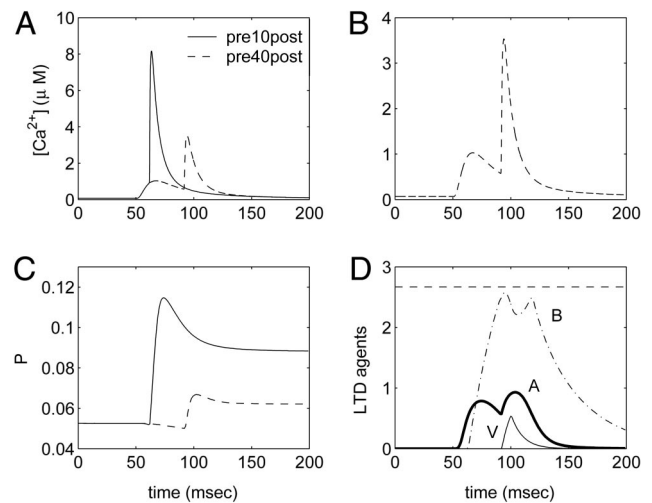


FIG. 5. Outcomes of single pre-post pairings show the mechanisms underlying pre-post plasticity. *A*: calcium time courses from pre-10-post (solid) and pre-40-post (dashed), as in Fig. 1A. *B*: magnified view of the calcium time course from pre-40-post from *A*. *C*: responses of the potentiation agent  $P$  to pre-10-post (solid) and pre-40-post (dashed) from the same initial level. *D*: responses of depression agents  $A$  (thick solid),  $B$  (dash-dotted), and the veto variable  $V$  to pre-40-post. Activation of  $V$  suppresses the response of  $B$  to the 2nd peak of  $A$ . As a result, the level of  $B$  fails to cross the threshold (dashed line) to activate the variable  $D$  and no depression occurs.

Figure 6 shows the differential activation of the depression components of our model under post-10-pre and post-60-pre protocols. We can observe in Fig. 6, *C* and *D*, that the depression agents respond to the calcium time course on different time scales. In Fig. 6*C*, corresponding to post-10-pre,  $B$  (dash-dotted) crosses the threshold (dashed line) to activate  $D$ . Figure 6*E* shows the response of  $D$  induced when  $B$  crosses the threshold by the amount shown in Fig. 6*C*. This response of  $D$  leads to strong depression. Figure 6*D* shows that the valley between the calcium peaks induced by pre- and postsynaptic stimulation, respectively (Fig. 6*B*, arrow), suppresses the  $B$  response in the post-60-pre case. The amount by which  $B$  crosses threshold in post-60-pre leads to a weak  $D$  response, shown in Fig. 6*F*, and only weak depression occurs. Note that the dashed line in Fig. 6, *E* and *F*, corresponds to  $D = 0.08$ , given as a reference since these two figures are on different scales. Note also that since the veto is not activated in these post-pre scenarios, it is not shown in Fig. 6, *C* and *D*.

An examination of the calcium time courses in Figs. 1, *C* and *D*, and 7, *A1* and *B1*, shows that small but distinct differences in the calcium profiles can be observed in the triplet pre-post-pre and post-pre-post triplet scenarios with 10-ms interstimulus intervals, relative to the pre-10-post case. Specifically, the pre-post-pre paradigm yields an additional calcium influx through NMDA channels due to the second presynaptic stimulation, which leads to the prolonged decay of calcium in Figs. 1*C* (arrow) and 7*A1*. In the post-pre-post case, the pre-post interaction is preceded by a calcium influx through VGCCs, and the pre-post itself leads to a slightly boosted calcium influx, relative to pre-10-post, as seen in Fig. 1*D*. As seen in Fig. 7*D*, the post-pre-post case activates the potentiation component  $P$  in our model but not the depression component  $D$ , whereas post-10-pre alone induces depression (Figs. 4 and 6). Thus post-pre-post leads to potentiation (Fig. 7*C*), as seen experimentally (Fig. 2). Depression is blocked in the post-pre-

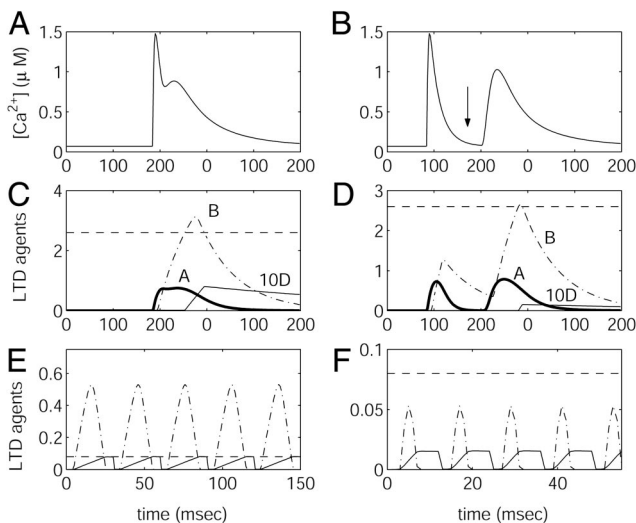


FIG. 6. Outcomes of single post-pre pairings. *A*: calcium time course from post-10-pre, as in Fig. 1*B*. *B*: calcium time course from post-60-pre, also as in Fig. 1*B*. Arrow emphasizes the “valley” of low calcium in this scenario. *C*: responses of depression agents *A* (thick solid), *B* (dash-dotted), and *D* (thin solid, multiplied by 10) to post-10-pre. Since *B* crosses the threshold value of 2.6 (dashed), *D* is induced to rise. *D*: responses to post-60-pre (coding as in *C*). Increase in *D* is negligible, leading to a weak effect on *W*. *E*: post-10-pre stimulation was applied 5 times at 1 Hz, and time periods during which *B* exceeded the threshold of 2.6 were concatenated. Dash-dotted curve shows *B*-2.6 during the concatenated periods, whereas the solid curve shows resulting rises in *D*. *F*: same experiment as in *E* was repeated with post-60-pre. Note the different scale from *E*. Dashed lines in *E* and *F* correspond to  $D = 0.08$ , the maximum value achieved by *D* in *E*.

post scenario by the veto, as can be seen in Fig. 7*B2*. The higher calcium level in the post-pre-post simulations than in the post-10-pre alone (Fig. 1, *B*-*D*) activates both this veto and *P*. We stress that the veto is included in the model for all simulations; it is the differences in calcium time course that lead to its activation in the post-pre-post case, but not in post-10-pre.

The pre-post-pre case, as seen in Figs. 1*C* and 7*A1*, has a similar calcium time course to pre-10-post and to post-pre-post but leads to no consistent synaptic plasticity (Figs. 7*C*, blue curve, and 2). As mentioned above, the distinctive feature of the pre-post-pre case is a slightly higher shoulder in the decaying phase of the calcium profile, relative to pre-10-post (Fig. 1*C*, arrow). This shoulder is enough to counteract the effects of the veto because the calcium level spends a sufficiently long time below the level needed for veto activation but still above the level needed to trigger depression, as seen in Fig. 7*A2*. The resulting activation of *D* offsets the simultaneously induced activation of *P* (Fig. 7*D*). This leads to a lack of preferred direction of change of the synapse (Fig. 7*C*). This clearly shows how finely tuned the detector must be so that the triplet interactions can be made consistent with the experiments. In DISCUSSION, we consider possibilities that may make the system more robust.

In addition to spike triplets, we compared the predictions of our model with recent experimental data on spike quadruplets (Wang et al. 2005) and found qualitative agreement for the same parameter values used in the pair and triplet simulations. As in the triplet case, different arrangements of spikes produced different plasticity results, with no obvious rule based on the spike times.

### Effects of active conductances in dendrites

It has been suggested that the outward potassium A-current plays a crucial role in STDP. Specifically, an EPSP may quickly and transiently inactivate the A-current, boosting the amplitude of a back-propagating AP that occurs just afterward (Magee and Johnston 1997; Migliore et al. 1999; Watanabe et al. 2002). The postsynaptic depolarization, and hence the extent of A-channel inactivation, depends on calcium influx, and the state of the A-channels in turn feeds back on calcium influx; although the A-channels do not themselves allow direct calcium influx, they are relevant to the postsynaptic calcium time course. Using published parameter values for the A-current, we find that blocking the A-current in the dendritic compartment has little qualitative effect on the STDP results produced by pre-post and post-pre stimulus pairs in our model.

A-current blockade does alter triplet results, however. Specifically, if the A-current is blocked in pre-post-pre simulations, then potentiation results. This potentiation occurs because the calcium influx via both L-type and NMDA calcium channels is increased. Higher calcium levels lead to stronger activation of the potentiation component of the model, and they also activate the veto more strongly. By the time the veto wears off, the calcium influx has returned to baseline levels. Thus the depression component of the model experiences only the usual activation, and the balance of LTP/LTD is tipped to favor potentiation. Post-pre-post simulations under A-current blockade still give potentiation. In post-pre-post simulations, the  $Mg^{2+}$  block of NMDA channels is fully removed by the

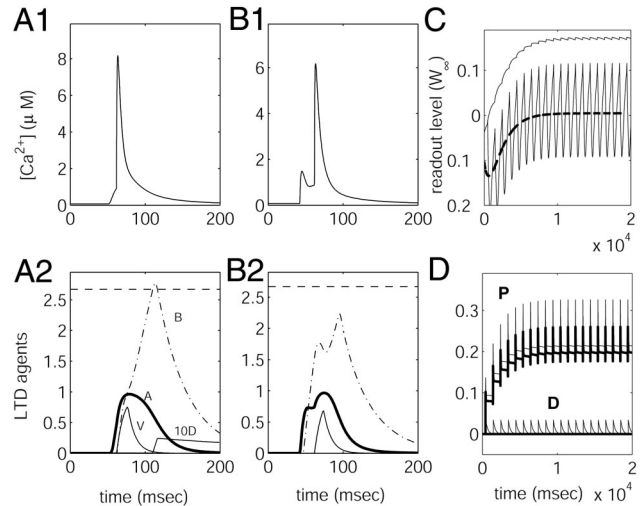


FIG. 7. Outcomes of spike triplets. *A*: model response to pre-post-pre. *A1*: calcium time course, as in Fig. 1*C*. *A2*: response of depression agents *A* (thick solid), *B* (dash-dotted), *D* (thin solid, multiplied by 10), and veto *V* (also thin solid) shows that, despite the rise in *V*, the slow decay of calcium allows *B* to cross the threshold (dashed) for *D* activation. *B*: model response to post-pre-post. *B1*: calcium time course, as in Fig. 1*D*. *B2*: response of depression agents *A* (thick solid) and *B* (dash-dotted) and veto *V* (thin solid) shows that *B* fails to cross threshold (thus *D* is negligible, and we omit it). *C*: plasticity outcomes are indicated by levels of the readout variable *W*. Pre-post-pre leads to oscillations of *W* (highly variable thin curve) about an average value  $\langle W \rangle = 0$  (thick curve), whereas post-pre-post (approximately monotonic thin curve) leads to positive *W*, corresponding to potentiation. *D*: In pre-post-pre (thin curves), the potentiation detector *P* (top curve) and the depression detector *D* (bottom curve) are both activated, leading to the cancellation that gives  $\langle W \rangle = 0$  in *C*. In post-pre-post (thick curves), there is less activation of *P* (top curve) than in pre-post-pre, but there is no activation of the *D* (bottom curve), and hence potentiation results.

second postsynaptic stimulation, even with the A-current intact, and thus A-current blockage has little effect on plasticity. In summary, A-current blockade leads to potentiation in both pre-post-pre and post-pre-post experiments, which matches the findings obtained in triplet experiments by Sjöström et al. (2001). This suggests that differences in densities of dendritic potassium channels may contribute to differences in plasticity outcomes of triplet experiments observed in different preparations.

Another experimental manipulation that has been performed in the context of STDP is the blockade of L-type calcium channels. Blocking L-type calcium channels in our model eliminates depression, but not potentiation, in the paired STDP protocol. This also agrees with the results seen in experiments (Bi and Poo 1998).

### Modular signaling for LTP and LTD

In recent experimental work on STDP in hippocampal culture, Wang et al. (2005) found that pharmacological block of CaMKII eliminates pre-post plasticity and leads to LTD in triplet paradigms. Complementing this result, blockade of calcineurin leads to no plasticity from post-pre pairings and LTD in triplet experiments (Wang et al. 2005). Corresponding alterations may be introduced in our model, based on its modular structure, and yield similar plasticity outcomes. In particular, blocking the growth of the LTP component  $P$  in our model eliminates pre-post plasticity, while blocking the rise of the initiator element  $A$  on the LTD side of our model eliminates post-pre plasticity and yields LTP from both pre-post-pre and post-pre-post triplet experiments (data not shown). However, in the case when  $P$  is blocked, the model does not reproduce the LTD observed experimentally in post-pre-post experiments, perhaps relating to an overly strong veto effect in the model.

### Presynaptic stimulation experiments yield a "No Man's Land"

In addition to matching STDP experiments, our model calcium detector yields results that are compatible with LTP/LTD induced by presynaptic stimulation under postsynaptic dendritic voltage clamp (Cho et al. 2001) (Fig. 8). In these experiments, 200 presynaptic stimuli are applied at 1 Hz. As the postsynaptic cell is held at progressively higher voltage levels, depression emerges, a "No Man's Land" (Lisman 2001) where there is no plasticity occurs at moderate voltages, and finally potentiation results at the most depolarized levels. Figure 8A shows this trend, as produced by our model. Furthermore, in experiments done with a voltage clamp to  $-10$  mV, increasing the concentration of a calcium buffer by a moderate amount switches potentiation to depression, while sufficiently large additional increases in buffer concentration eliminate plasticity (Cho et al. 2001). Our model also reproduces this result at any level of voltage clamping at which potentiation occurs at default buffer concentrations (Fig. 8B).

Figure 8C shows that our model yields the expected switch-over from LTD to LTP in experiments with repeated presynaptic stimulation, as the stimulation frequency increases (Dudek and Bear 1992; Wang and Wagner 1999). While the result shown in Fig. 8C was obtained under postsynaptic

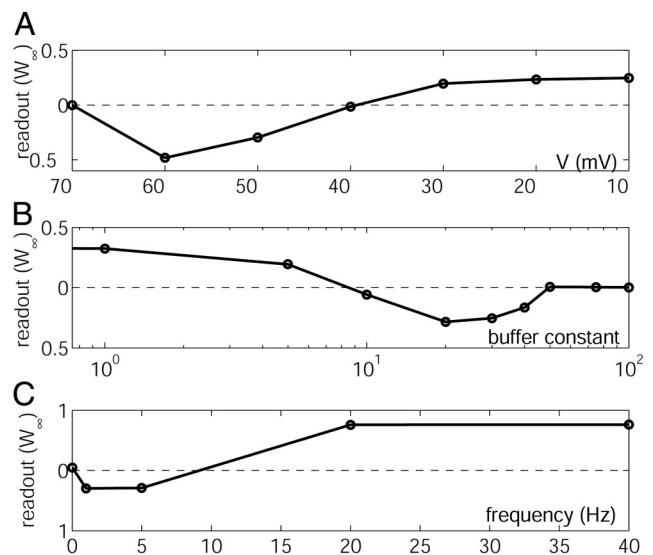


FIG. 8. Potentiation/depression results from presynaptic stimulation under postsynaptic voltage clamp. *A*: saturated readout ( $W_\infty$ ) levels after 200 presynaptic stimuli delivered at 1 Hz, with the postsynaptic cell voltage clamped to the voltages shown. *B*: saturated readout ( $W_\infty$ ) levels from 200 presynaptic stimuli given at 1 Hz with postsynaptic voltage clamp to  $-10$  mV and with the model buffer constant  $\beta_{\text{buff}}$  ranging over the levels shown. *C*: saturated readout ( $W_\infty$ ) levels from repeated presynaptic stimulation at the frequencies shown, with postsynaptic voltage clamp to  $-40$  mV.

voltage clamp, an analogous crossover occurs without the clamp. Without voltage clamp, we find that the crossover frequency decreases as we increase the AMPA conductance (data not shown), which must be considered as an unknown parameter for these particular simulations, since switchover experiments in hippocampal slices were performed using extracellular field EPSPs to drive the postsynaptic cell (Wang and Wagner 1999). Similar crossover results, which have been likened to the BCM sliding threshold rule (Bienenstock et al. 1982), have been shown in several earlier STDP models (Abarbanel et al. 2002; Izhikevich and Desai 2003; Senn et al. 2001; Shouval et al. 2002).

Finally, to show further the role of postsynaptic calcium in LTP/LTD, we examined the consequences of depolarization of the model postsynaptic cell to 0 mV, in the absence of presynaptic stimulation. Our model reproduces the experimental finding (Conti and Lisman 2002; Malenka et al. 1988) that this paradigm leads to no plasticity. In the model, postsynaptic depolarization to 0 mV inactivates VGCCs, preventing sufficient calcium influx for the induction of plasticity.

The similarity between the results produced by our calcium detector model (e.g., Fig. 8) and those seen experimentally is consistent with the idea that STDP and classical LTP/LTD share similar intracellular mechanisms.

### DISCUSSION

We show that a detector system that is sensitive to certain temporal aspects of the calcium time course can distinguish between pair and triplet pre- and postsynaptic stimulation scenarios and is consistent with classical LTP/LTD experiments. We show additionally that any detector system that only considers calcium levels (as in previous plasticity models) cannot reconcile all of this experimental data.

Examination of the calcium time course across different scenarios indicates that a calcium time course detector system should incorporate three rules: 1) a high threshold for potentiation, 2) a combined low-amplitude, long-duration signal detector for depression, and 3) a mid-level veto of depression. While calcium levels still play a role in this system, the latter two ingredients in particular yield a strong dependence on temporal dynamics of the calcium signal. Furthermore, we have shown that for a detector that is sensitive only to calcium levels, depression in pre-post scenarios with large interstimulus intervals is unavoidable. This phenomenon, which is not supported by experiments, does not arise in our model. While the calcium time course detector in this work uses a small number of elements to convert the above rules into accurate reproductions of plasticity outcomes across experimental scenarios, this success requires some degree of fine-tuning. The similarity of calcium time courses seen in our simulations, across scenarios that yield different plasticity outcomes in experiments, suggests that variability in plasticity outcomes from the repeated application of certain experimental protocols will be inevitable in a calcium-based system.

*Veto mechanism eliminates pre-post depression with calcium time course detection but not with level detection*

Note that the ability of our detector to eliminate the depression seen in other models when the presynaptic stimulation precedes the postsynaptic stimulation by a long time interval follows because the depression trigger is a time course detector composed of three elements, rather than a simple level detector. In our model, in addition to contributing to the absence of pre-post depression, the veto prevents depression in the post-pre-post case and is responsible for the “No Man’s Land” for intermediate levels of calcium in the classical LTP/LTD protocol of Cho et al. (2001) (Fig. 8). In the latter case, the veto works to limit the response of the depressive elements in the model, such that a cancellation between depression and potentiation occurs.

It is important to note that, in a pure calcium level detection model for STDP, the presence of a veto is still not sufficient to eliminate pre-post depression with large interstimulus intervals. This is because as the time interval between pre- and postsynaptic events increases, the calcium level must necessarily fall (Fig. 1A) (Karmarkar and Buonomano 2002). Eventually, the calcium triggered by the pre-post stimuli will fall to the level found in the post-10-pre case, which causes depression. Thus at this level, the veto will not be activated, and depression will occur. The calcium time course detector avoids this outcome because when the calcium level falls to such a low level, its time course is no longer broad enough to trigger depression.

In theory, the lack of consistent synaptic conductance changes observed experimentally in the pre-post-pre case could result from unreliable synaptic transmission. Specifically, release failure in pre-post-pre experiments could effectively yield a sequence of pre-post and post-pre events leading to a cancellation between potentiation and depression signals. As the modulation of release probability is responsible for synaptic depression and facilitation, this idea could explain some of the variability in outcomes of pre-post-pre experiments in terms of differing biases toward paired-pulse depression or facilitation

within different presynaptic cells. However, although the presynaptic release probability in these cultures has not been measured directly, most synapses studied here display weak synaptic depression and facilitation, and preliminary results suggest that outcomes of pre-post-pre experiments in culture are independent of these short-term plasticity features of the presynaptic cell (Wang et al. 2005). This leads us to favor the idea that pre-post-pre variability derives at least in part from heterogeneity in parameters associated with postsynaptic calcium time-course detection rather than presynaptic effects alone.

*Sensitivity of calcium time course detection implies variability in plasticity outcomes*

Our model detector system distinguishes between the various calcium time courses of pre- and postsynaptic spike pairs and triplets, eliminates depression in pre-post scenarios with large interstimulus intervals, and matches classical LTP/LTD experiments. However, it also requires fine-tuning. To ensure that pre-post-pre produces no preferred direction of synaptic change, the balance between the veto level and the depression trigger must be precisely set. Small changes in neuronal excitability, such as altering the strength of the A-current or the AHP current, can alter the results. These seem to be unavoidable aspects of any detector system that distinguishes between calcium time courses induced in the pre-post, post-pre, and triplet scenarios, as evidenced by the similarity of the calcium time courses appearing in these scenarios, seen in Fig. 1. The sensitivity of the detector leads us to conclude that responses to multi-spike patterns cannot be universal and consistent across all synapses if changes in synaptic strengths are based exclusively on a calcium signal coming from NMDA channels and VGCCs (see also Ismailov et al. 2004; Saudargiene et al. 2004). Future experiments that examine the dependence of STDP outcomes on synaptic location within the dendritic tree would provide a further test of the nature of this variability. This conclusion is also in keeping with the variability seen across systems in which spike pairings (reviewed in Abbott and Nelson 2000) or multiple spike interactions (Froemke and Dan 2002; Sjöström et al. 2001; Wang et al. 2005) have been explored; however, differences in plasticity outcomes across preparations likely also depend on differences in features, such as short-term plasticity and regulation of BPAPs, across these preparations.

*Possible mechanisms for added robustness*

The sensitivity of our model to changes in certain parameters may relate to the experimentally observed variability in STDP outcomes for each fixed protocol (e.g., Bi and Poo 1998; Wang et al. 2005) (Fig. 2). On the other hand, there may be ways to augment the calcium signal in the model to add robustness to a system that converts calcium time courses into synaptic plasticity outcomes. For example, calcium is heavily buffered in the dendrite, and it has been proposed that spatial separation of calcium entering through NMDA channels versus the VGCCs could simplify the spike-time detector (Karmarkar and Buonomano 2002). While there is experimental evidence that calcium is spatially isolated within a spine (Nimchinsky et al. 2002; Sabatini et al. 2002), the evidence for further localization

to areas inside the spine is inconclusive. Furthermore, our computational analysis indicates that models based on spatial separation of calcium still require a significant amount of fine-tuning to account for all the STDP data sets. The separation hypothesis suggests that synaptic NMDA calcium ( $I_{CaS}$ ) induces potentiation, whereas depression stems from the interaction of VGCC calcium ( $I_{CaL}$ ) with  $I_{CaS}$  or some other agent. This second component is needed to account for the fact that  $I_{CaL}$  levels are similar in depressing post-pre and nondepressing post-alone scenarios. Without a veto, models based on separation, with interaction of  $I_{CaL}$  and  $I_{CaS}$  for depression, lead to depression in pre-post scenarios with long interstimulus intervals (data not shown), exactly as seen in our model when the veto is omitted and in other calcium-based models (Abarbanel et al. 2003; Shouval et al. 2002). Karmarkar and Buonomano (2002) circumvent this issue by attributing depression to the interaction of  $I_{CaL}$  with metabotropic glutamate receptors, which they postulate are inactive in pre-post scenarios; this amounts to imposing a veto on depression in all pre-post interactions. However, this implies that there is an additional mechanism that is able to distinguish between pre-post and post-pre pairings. Even with a veto, spatial separation models still require some tuning. In particular, when the veto activation threshold is lowered sufficiently to prevent depression in the pre-40-post case, fine-tuning is required to allow enough depression to occur to cancel potentiation in the pre-post-pre case. Nonetheless, because of the myriad of possible ways to implement calcium detection with spatially separated calcium sources, their role in shaping plasticity merits attention in future work.

An important calcium source that we have not explicitly modeled is calcium release by intracellular calcium stores, which has been implicated as possibly contributing to depression. The decision not to treat this factor directly was motivated by the fact that the release from these stores has been found to be slow compared with the time scales required to resolve STDP (Kovalchuk et al. 2000; Sabatini et al. 2002), and blockade of calcium-induced calcium release does not significantly affect calcium influx in postsynaptic spines (Kovalchuk et al. 2000). Furthermore, since we selected parameter values relevant to calcium dynamics to match experimental observations of calcium signals (Koester and Sakmann 1998; Murthy et al. 2000; Sabatini et al. 2002), any short-term effects of calcium stores are implicitly encoded in the dynamics of our model. Longer-term effects of stores, which may be relevant for consolidating the effects of potentiation and depression, have been neglected.

Finally, it is also possible that stochasticity in the calcium dynamics due to small numbers of calcium ions in the spine contributes significantly to STDP in some systems. It has recently been shown (Shouval and Kalantzis 2005) that stochasticity may lessen depression at long pre-post intervals in a model based on calcium levels alone. However, it is not yet known how this model could be adjusted to reproduce the experimental results with triplet stimulation (Fig. 2), given the extreme similarity of peak calcium levels in pre-post, pre-post-pre, and post-pre-post scenarios (Fig. 1). Furthermore, the inclusion of stochasticity in the dynamics of calcium in our model has little impact on plasticity outcomes.

### Generality of results

The arguments given here support the idea that calcium levels alone cannot be used to distinguish experimentally observed spike pair and triplet results, independent of modeling issues. Using a biophysical CA1 cell representation (Poirazi et al. 2003) to simulate calcium time courses, we examined whether there is enough information in the calcium time course in itself to distinguish various STDP protocols. We found that this should be the case provided three basic rules are observed. We then constructed a postsynaptic calcium time course detector that implements these rules. This detector system is based on the pathways influencing CaMKII regulation (Bhalla and Iyengar 1999; Lisman 2001). There may be alternative means of constructing such a detector but our analysis suggests that all of its qualitative features are necessary in the absence of additional assumptions. To keep our model as simple as possible, we did not attempt to derive a detailed biophysical model of the molecular pathways that respond to calcium signals. Our intention was to show feasibility and plausibility of a calcium time course detector. However, employing more biological realism may be worthwhile in the future.

We adapted an experimentally calibrated CA1 model for this work. It is possible that some differences may arise between the precise dynamics of cultured CA1 neurons and the dynamics of neurons in the *in vitro* preparations used in the calibration of the CA1 model. However, the details of the parameter choices and the number of compartments in our model are actually not important for our overall conclusions, namely that there is enough information in the postsynaptic calcium time course to distinguish the various scenarios of STDP, but any mechanism of synaptic plasticity based on this signal is necessarily sensitive to parameter changes. The essential feature of any calcium detection system is the interaction of NMDA channels with back-propagating action potentials. The magnesium block is the key timing element for the system. As a result, as long as this feature is captured qualitatively, inaccuracies in the parameters of our model can be tolerated without significantly altering our findings. Moreover, as long as we choose a reasonable coupling parameter between the somatic and dendritic compartments, the amplitude of the BPAP arriving in the model dendrite should be compatible with that of *some* point on the dendritic tree of a CA1 pyramidal cell (Holthoff et al. 2002; Saudargiene et al. 2004). We also note that changes in the buffering rates of calcium in the model, to first approximation, yield a compression or expansion of our calcium time courses. This scaling affects the tuning required of the detector, but the qualitative plasticity outcomes remain unchanged (Fig. 9A). Finally, it is important to note that the sensitivity in our model is *not* a sensitivity to noise in spike timing. Indeed, our plasticity outcomes are robust to spike timing jitter (Fig. 9B).

There are other mechanisms that a neuron may use to translate a combination of pre- and postsynaptic spike timing into cellular signals leading to synaptic modification. Recent experiments on neocortical layer 5 pyramidal cell pairs indicate that in that system, the coincident activation of presynaptic NMDA and cannabinoid receptors may induce LTD in a spike-timing-dependent manner (Sjöström et al. 2003). However, at low frequencies of paired stimulation, including 0.1

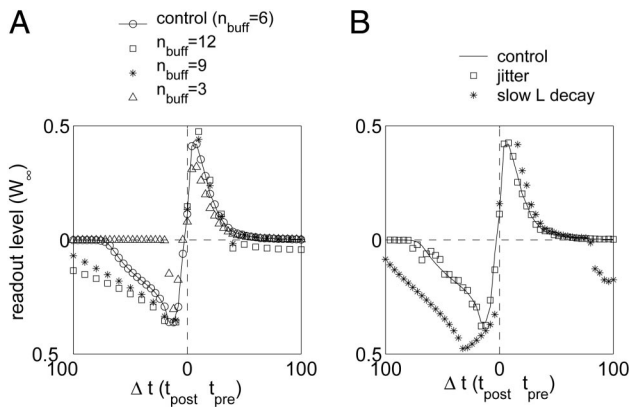


FIG. 9. STDP induction depends on model parameters and features. *A*: changes in calcium buffering rates ( $n_{\text{buff}}$ ) compress or expand plasticity outcomes. Saturated readout levels ( $W_\infty$ ) are shown for spike pair experiments with interspike intervals  $\Delta t = t_{\text{post}} - t_{\text{pre}}$ . Control curve is the same curve shown in Fig. 4. *B*: plasticity outcomes are robust to jitter in spike timing but depend on the decay rate of voltage-gated calcium channels (VGCCs). For the jitter results, the  $n$ th postsynaptic spike was induced at time  $t_{\text{post}} + j_n$ , where each  $j_n$  was selected randomly from a normal distribution with mean 0 and SD 1/10th the absolute value of  $t_{\text{post}} - t_{\text{pre}}$ . For slow *L* decay, the decay rate of the L-type calcium current was slowed, with an adjustment to ensure little change in calcium influx rate and peak calcium levels.

and 5 Hz, this cannabinoid mechanism alone is insufficient to account for timing-dependent LTD. Meanwhile, the importance of postsynaptic mechanisms has been stressed by numerous results on classical LTP and LTD, as well as experimental findings that postsynaptic calcium elevation is necessary for hippocampal STDP (Li et al. 2004). It will be interesting to see whether future experiments will uncover a presynaptic component of STDP in hippocampal preparations, given that plasticity outcomes of spike triplet experiments differ across different preparations (Froemke and Dan 2002; Sjöström et al. 2001; Wang et al. 2005) (Fig. 2). If so, presynaptic components of STDP may also be incorporated into the framework of our model in future work, perhaps with modifications to take into account additional time scales of signaling.

#### Predictions and consequences for synaptic computations

The results of Sjöström et al. (2001), Froemke and Dan (2002), and our work suggest that a universal plasticity rule for trains of multiple spikes based exclusively on spike times may not exist. In particular, the experiments do not support a rule based on a linear combination of pairs of spikes, as suggested by several elegant STDP models (Abarbanel et al. 2002, 2003; Karbowski and Ermentrout 2002; Karmarkar and Buonomano 2002). While these models could be adjusted to account for the multi-spike experiments of Sjöström et al. (2001), they would be more hard-pressed to account for the findings of Froemke and Dan (2002) or for our spike triplet results. Our triplet results are also not captured by computational studies in which pre-post-pre and post-pre-post outcomes are symmetric (Abarbanel et al. 2003).

In our model, A-current blockade can lead to potentiation in both pre-post-pre and post-pre-post experiments (Sjöström et al. 2001). Furthermore, our model supports the idea that LTP or LTD can be unmasked in pre-post-pre experiments (Wang et al. 2005) and that they can cancel in experiments invoking plasticity using presynaptic stimulation with postsynaptic volt-

age clamp (Cho et al. 2001). Conversely, we predict that if precisely timed caged calcium release could be used to bolster calcium levels during the decay phase of a pre-post or post-pre-post experiment, so that the calcium time course was converted to that of the pre-post-pre scenario, LTP could be canceled. Our analysis also predicts the existence of a molecular veto mechanism that is harnessed by calcium signals above a moderate threshold to suppress LTD. Finally, our model suggests that slowing the decay rate of the L-type VGCCs, while simultaneously adjusting parameters to maintain calcium influx rate and peak calcium levels, would lead to pre-post-pre LTP, because the resulting broadening of the calcium signal above the LTP threshold would dominate over that below the LTP threshold (data not shown). This slowing would also broaden the LTD window in post-pre spike pair experiments and introduce LTD under pre-post with long interspike intervals, where the LTP module is not activated, due to a prolonged calcium time course (Fig. 9B).

The dependence of synaptic plasticity on calcium time course would lead to two additional computational consequences. First, plasticity outcomes induced by similar stimuli would not be consistent across all synapses and neural systems, but would depend on the specific properties of the local calcium, synaptic, and membrane kinetics. For example, local increases in dendritic excitability tend to promote LTP in pre-post-pre scenarios in our model while broadening the LTD window in spike pair experiments (data not shown). Second, synaptic plasticity contingent on calcium time course would display an enhanced sensitivity to the precise temporal details of spike trains, relative to plasticity based on levels alone. This added acuity could enable synaptically connected circuits to learn to differentiate more intricate sequences of spike times.

#### ACKNOWLEDGMENTS

We thank H. Wang for kindly providing original data of triplet experiments. We are grateful to A. Barth, F. Thiels, and N. Urban for careful reading and useful comments on an earlier draft of this manuscript.

#### GRANTS

This work was partially supported by National Science Foundation Grants DMS-0108857 and DMS-0414023 to J. E. Rubin, a Career Award in the Biomedical Sciences from the Burroughs Wellcome Fund to G. Bi, National Institute of Mental Health Grants R01 MH-066962 to G. Bi and K01-MH-01508 and P50-MH-64445 to C. C. Chow, and an award from the A. P. Sloan Foundation to C. C. Chow.

#### REFERENCES

- Abarbanel HD, Gibb L, Huerta R, and Rabinovich MI. Biophysical model of synaptic plasticity dynamics. *Biol Cybern* 89: 214–226, 2003.
- Abarbanel HD, Huerta R, and Rabinovich MI. Dynamical model of long-term synaptic plasticity. *Proc Natl Acad Sci USA* 99: 10132–10137, 2002.
- Abbott LF and Nelson SB. Synaptic plasticity: taming the beast. *Nat Neurosci Suppl* 3: 1178–1183, 2000.
- Aihara T, Abiru Y, Kashiwagi Y, Ymazaki Y, and Tsukada M. Ca<sup>2+</sup> influx during the induction of the spike-timing dependent plasticity in the hippocampal CA1 network. *Neurosci Res* 46: S175, 2003.
- Andrasfalvy BK and Magee JC. Distance-dependent increase in AMPA receptor number in the dendrites of adult hippocampal CA1 pyramidal neurons. *J Neurosci* 21: 9151–9159, 2001.
- Bell CC, Han VZ, Sugawara Y, and Grant K. Synaptic plasticity in a cerebellum-like structure depends on temporal order. *Nature* 387: 278–281, 1997.
- Bhalla US and Iyengar R. Emergent properties of networks of biological signaling pathways. *Science* 283: 381–387, 1999.

- Bi GQ.** Spatiotemporal specificity of synaptic plasticity: cellular rules and mechanisms. *Biol Cybern* 87: 319–332, 2002.
- Bi G-Q and Poo M-M.** Synaptic modifications in cultured hippocampal neurons: dependence on spike timing, synaptic strength, and postsynaptic cell type. *J Neurosci* 18: 10464–10472, 1998.
- Bi GQ and Poo M-M.** Synaptic modification by correlated activity: Hebb's postulate revisited. *Annu Rev Neurosci* 24: 139–166, 2001.
- Bi GQ and Wang HX.** Temporal asymmetry in spike timing-dependent synaptic plasticity. *Physiol Behav* 77: 551–555, 2002.
- Bienenstock EL, Cooper LN, and Munro PW.** Theory for the development of neuron selectivity: Orientation specificity and binocular interaction in visual cortex. *J Neurosci* 2: 32–48, 1982.
- Bradshaw JM, Kubota Y, Meyer T, and Schulman H.** An ultrasensitive  $\text{Ca}^{2+}$ /calmodulin-dependent protein kinase II-protein phosphatase 1 switch facilitates specificity in postsynaptic calcium signaling. *Proc Natl Acad Sci USA* 100: 10512–10517, 2003.
- Cho K, Aggleton JP, Brown MW, and Bashir ZI.** An experimental test of the role of postsynaptic calcium levels in determining synaptic strength using perirhinal cortex of rat. *J Physiol* 532: 459–466, 2001.
- Conti R and Lisman J.** A large sustained  $\text{Ca}^{2+}$  elevation occurs in unstimulated spines during the LTP pairing protocol but does not change synaptic strength. *Hippocampus* 12: 667–679, 2002.
- Debanne D, Gahwiler BH, and Thompson SM.** Long-term synaptic plasticity between pairs of individual CA3 pyramidal cells in rat hippocampal slice cultures. *J Physiol* 507: 237–247, 1998.
- Dudek SM and Bear MF.** Homosynaptic long-term depression in area CA1 of hippocampus and effects of *N*-methyl-D-aspartate receptor blockade. *Proc Natl Acad Sci USA* 89: 4363–4367, 1992.
- Ermentrout B.** *Simulating, Analyzing, and Animating Dynamical Systems*. Philadelphia: SIAM, 2002.
- Froemke RC and Dan Y.** Spike-timing-dependent synaptic modification induced by natural spike trains. *Nature* 416: 433–438, 2002.
- Goldberg JH, Tamas G, Aronov D, and Yuste R.** Calcium microdomains in aspiny dendrites. *Neuron* 40: 807–821, 2003.
- Holmes WR.** Models of calmodulin trapping and CaM kinase II activation in a dendritic spine. *J Comput Neurosci* 8: 65–85, 2000.
- Holthoff K, Tsay D, and Yuste R.** Calcium dynamics of spines depend on their dendritic location. *Neuron* 33: 425–437, 2002.
- Ismailov I, Kalikulov D, Inoue T, and Friedlander MJ.** The kinetic profile of intracellular calcium predicts long-term potentiation and long-term depression. *J Neurosci* 24: 9847–9861, 2004.
- Izhikevich EM and Desai NS.** Relating STDP to BCM. *Neural Comp* 15: 1511–1523, 2003.
- Jahr CE and Stevens CF.** A quantitative description of NMDA receptor-channel kinetic behavior. *J Neurosci* 10: 1830–1837, 1990.
- Jahr CE and Stevens CF.** Calcium permeability of the *N*-methyl-D-aspartate receptor channel in hippocampal neurons in culture. *Proc Natl Acad Sci USA* 90: 11573–11577, 1993.
- Karbowski J and Ermentrout GB.** Synchrony arising from a balanced synaptic plasticity in a network of heterogeneous neural oscillators. *Phys Rev E Stat Nonlin Soft Matter Phys* 65: 031902, 2002.
- Karmarkar UR and Buonomano DV.** A model of spike-timing dependent plasticity: one or two coincidence detectors? *J Neurophysiol* 88: 507–513, 2002.
- Koester HJ and Sakmann B.** Calcium dynamics in single spines during coincident pre- and postsynaptic activity depend on relative timing of back-propagating action potentials and subthreshold excitatory postsynaptic potentials. *Proc Natl Acad Sci USA* 95: 9596–9601, 1998.
- Kovalchuk Y, Eilers J, Lisman J, and Konnerth A.** NMDA receptor-mediated subthreshold  $\text{Ca}^{2+}$  signals in spines of hippocampal neurons. *J Neurosci* 20: 1791–1799, 2000.
- Lee HK, Barbarosie M, Kameyama K, Bear MF, and Huganir RL.** Regulation of distinct AMPA receptor phosphorylation sites during bidirectional synaptic plasticity. *Nature* 405: 955–959, 2000.
- Li C-Y, Lu J-T, Wu C-P, Duan S-M, and Poo M-M.** Bidirectional modification of presynaptic neuronal excitability accompanying spike timing-dependent synaptic plasticity. *Neuron* 41: 257–268, 2004.
- Lisman J.** A mechanism for the Hebb and the anti-Hebb processes underlying learning and memory. *Proc Natl Acad Sci USA* 86: 9574–9578, 1989.
- Lisman J.** The CaM kinase II hypothesis for the storage of synaptic memory. *Trends Neurosci* 17: 406–412, 1994.
- Lisman J, Schulman H, and Cline H.** The molecular basis of CaMKII function in synaptic and behavioural memory. *Nat Rev Neurosci* 3: 175–190, 2002.
- Lisman JE.** Three  $\text{Ca}^{2+}$  levels affect plasticity differently: the LTP zone, the LTD zone and no man's land. *J Physiol* 532: 285, 2001.
- Lisman JE and Zhabotinsky AM.** A model of synaptic memory: a CaMKII/PP1 switch that potentiates transmission by organizing an AMPA receptor anchoring assembly. *Neuron* 31: 191–201, 2001.
- Magee JC and Johnston D.** A synaptically controlled, associative signal for Hebbian plasticity in hippocampal neurons. *Science* 275: 209–213, 1997.
- Malenka RC, Kauer JA, Perkel DJ, Mauk MD, Kelly PT, Nicoll RA, and Waxham MN.** An essential role for postsynaptic calmodulin and protein kinase activity in long-term potentiation. *Nature* 340: 554–557, 1989.
- Malenka RC, Kauer JA, Zucker RS, and Nicoll RA.** Postsynaptic calcium is sufficient for potentiation of hippocampal synaptic transmission. *Science* 242: 81–84, 1988.
- Malinow R, Schulman H, and Tsien RW.** Inhibition of postsynaptic PKC or CaMKII blocks induction but not expression of LTP. *Science* 245: 862–866, 1989.
- Maravall M, Mainen ZF, Sabatini BL, and Svoboda K.** Estimating intracellular calcium concentrations and buffering without wavelength ratioing. *Biophys J* 78: 2655–2667, 2000.
- Markram H, Luebke J, Frotscher M, and Sakmann B.** Regulation of synaptic efficacy by coincidence of postsynaptic APs and EPSPs. *Science* 275: 213–215, 1997.
- Migliore M, Hoffman DA, Magee JC, and Johnston D.** Role of an A-type  $\text{K}^{+}$  conductance in the back-propagation of action potentials in the dendrites of hippocampal pyramidal neurons. *J Comput Neurosci* 7: 5–15, 1999.
- Mulkey RM, Endo S, Shenolikar S, and Malenka RC.** Involvement of a calcineurin/inhibitor-1 phosphatase cascade in hippocampal long-term depression. *Nature* 369: 486–488, 1994.
- Murthy VN, Sejnowski TJ, and Stevens CF.** Dynamics of dendritic calcium transients evoked by quantal release at excitatory hippocampal synapses. *Proc Natl Acad Sci USA* 97: 901–906, 2000.
- Nimchinsky EA, Sabatini BL, and Svoboda K.** Structure and function of dendritic spines. *Annu Rev Physiol* 64: 313–353, 2002.
- Nishiyama M, Hong K, Mikoshiba K, Poo MM, and Kato K.** Calcium stores regulate the polarity and input specificity of synaptic modification. *Nature* 408: 584–588, 2000.
- Perouansky M and Yaari Y.** Kinetic properties of NMDA receptor-mediated synaptic currents in rat hippocampal pyramidal cells versus interneurons. *J Physiol* 465: 223–244, 1993.
- Poirazi P, Brannon T, and Mel BW.** Arithmetic of subthreshold synaptic summation in a model CA1 pyramidal cell. *Neuron* 37: 977–987, 2003.
- Pozzo-Miller LD, Pivovarova NB, Connor JA, Reese TS, and Andrews B.** Correlated measurements of free and total intracellular calcium concentration in central nervous system neurons. *Mic Res Tech* 46: 370–379, 1999.
- Sabatini BL, Oertner TG, and Svoboda K.** The life cycle of  $\text{Ca}^{2+}$  ions in dendritic spines. *Neuron* 33: 439–452, 2002.
- Saudargienne A, Porr B, and Worgotter F.** How the shape of pre- and postsynaptic signals can influence STDP: a biophysical model. *Neural Comp* 16: 595–625, 2004.
- Senn W.** Beyond spike timing: the role of nonlinear plasticity and unreliable synapses. *Biol Cybern* 87: 344–355, 2002.
- Senn W, Markram H, and Tsodyks M.** An algorithm for modifying neurotransmitter release probability based on pre- and postsynaptic spike timing. *Neural Comput* 13: 35–67, 2001.
- Shouval HZ, Bear MF, and Cooper LN.** A unified model of NMDA receptor-dependent bidirectional synaptic plasticity. *Proc Natl Acad Sci USA* 99: 10831–10836, 2002.
- Shouval HZ and Kalantzis G.** Stochastic properties of synaptic transmission affect the shape of spike time-dependent plasticity curves. *J Neurophysiol* 93: 1069–1073, 2005.
- Sjöström PJ and Nelson SB.** Spike timing, calcium signals and synaptic plasticity. *Curr Opin Neurobiol* 12: 305–314, 2002.
- Sjöström PJ, Turrigiano GG, and Nelson SB.** Rate, timing, and cooperativity jointly determine cortical synaptic plasticity. *Neuron* 32: 1149–1164, 2001.
- Sjöström PJ, Turrigiano GG, and Nelson SB.** Neocortical LTD via coincident activation of presynaptic NMDA and cannabinoid receptors. *Neuron* 39: 641–654, 2003.
- Togashi K, Kitajima T, Aihara T, Hong K, Poo M, and Nishiyama M.** Gating of activity-dependent long-term depression by GABAergic activity in the hippocampus. *Soc Neurosci Abstr* 123.4, 2003.
- Traub RD, Jefferys JG, Miles R, Whittington MA, and Toth K.** A branching dendritic model of a rodent CA3 pyramidal neurone. *J Physiol* 481: 79–95, 1994.

- Wang H and Wagner JJ.** Priming-induced shift in synaptic plasticity in the rat hippocampus. *J Neurophysiol* 82: 2024–2028, 1999.
- Wang H-X, Gerkin RC, Nauen DW, and Bi G-Q.** Coactivation and timing-dependent integration of synaptic potentiation and depression. *Nature Neurosci* 8: 187–193, 2005.
- Watanabe S, Hoffman DA, Migliore M, and Johnston D.** Dendritic K<sup>+</sup> channels contribute to spike-timing dependent long-term potentiation in hippocampal pyramidal neurons. *Proc Natl Acad Sci USA* 99: 8366–8371, 2002.
- Yang SN, Tang YG, and Zucker RS.** Selective induction of LTP and LTD by postsynaptic [Ca<sup>2+</sup>] elevation. *J Neurophysiol* 81: 781–787, 1999.
- Yao H and Dan Y.** Stimulus timing-dependent plasticity in cortical processing of orientation. *Neuron* 32: 315–323, 2001.
- Yuste R, Majewska A, Cash SS, and Denk W.** Mechanisms of calcium influx into hippocampal spines: heterogeneity among spines, coincidence detection by NMDA receptors, and optical quantal analysis. *J Neurosci* 19: 1976–1987, 1999.
- Zhabotinsky AM.** Bistability in the Ca(2+)/calmodulin-dependent protein kinase-phosphatase system. *Biophys J* 79: 2211–2221, 2000.
- Zhang LI, Tao HW, Holt CE, Harris WA, and Poo M.** A critical window for cooperation and competition among developing retinotectal synapses. *Nature* 395: 37–44, 1998.